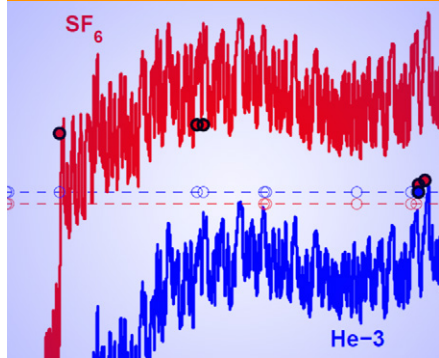


## Original Research



Underground nuclear tests may have late-time gas seepage to the surface, driven by barometric pumping. We use numerical models to investigate the effects of uncertainties in rock properties and season of detonation on estimates of gas breakthrough. These research results help predict the timing and window of opportunity for  $^{133}\text{Xe}$  detection.

A.B. Jordan, P.H. Stauffer, and G.A. Zvoloski, Computational Earth Sciences Group, Los Alamos National Lab., Los Alamos, NM 87545; J.K. MacCarthy and D.N. Anderson, Solid Earth Geophysics Group, Los Alamos National Lab., Los Alamos, NM 87545; and M.A. Person, Dep. of Earth and Environmental Science, New Mexico Tech, 801 Leroy Place, Socorro, NM 87801. \*Corresponding author (ajordan@lanl.gov).

Vadose Zone J.  
doi:10.2136/vzj2014.06.0070  
Received 13 June 2014.

© Soil Science Society of America  
5585 Guilford Rd., Madison, WI 53711 USA.

All rights reserved. No part of this periodical may be reproduced or transmitted in any form or by any means, electronic or mechanical, including photocopying, recording, or any information storage and retrieval system, without permission in writing from the publisher.

# Uncertainty in Prediction of Radionuclide Gas Migration from Underground Nuclear Explosions

Amy B. Jordan,\* Philip H. Stauffer, George A. Zvoloski, Mark A. Person, Jonathan K. MacCarthy, and Dale N. Anderson

Underground nuclear explosions (UNEs) produce radionuclide gases that may seep to the surface over weeks to months. The objective of this research was to quantify the impact of uncertainties in hydrologic parameters (fracture aperture, matrix permeability, porosity, and saturation) and season of detonation on the timing of gas breakthrough. Numerical sensitivity analyses were performed, with barometric pumping providing the primary driving force for gas migration, for the case of a 1 kt UNE at 400-m depth of burial. Gas arrival time was most affected by matrix permeability and fracture aperture. Gases having higher diffusivity were more sensitive to uncertainty in the rock properties. The effect of seasonality in the barometric pressure forcing was found to be important, with detonations in March the least likely to be detectable based on barometric data for Rainier Mesa, Nevada. Monte Carlo realizations were performed with all four parameters varying simultaneously to determine their interrelated effects. The Monte Carlo method was also used to predict the window of opportunity for  $^{133}\text{Xe}$  detection from a 1 kt UNE at Rainier Mesa, with and without matching the model to  $\text{SF}_6$  and  $^3\text{He}$  data from the 1993 Non-Proliferation Experiment. Results from the data-blind Monte Carlo simulations were similar but were biased toward earlier arrival time and less likely to show detectable  $^{133}\text{Xe}$ . The estimated timing of gas arrival may be used to deploy personnel and equipment to the site of a suspected UNE, if allowed under the terms of the Comprehensive Nuclear Test-Ban Treaty.

Abbreviations: CTBT, Comprehensive Nuclear-Test-Ban Treaty; FEHM, Finite Element Heat and Mass transfer code; NNSS, Nevada National Security Site; NPE, Non-Proliferation Experiment; UNE, underground nuclear explosion; VOC, volatile organic compound.

In the event of a clandestine underground nuclear test, evidence of signature radionuclide gases could help verify the nuclear nature of the event. The Comprehensive Nuclear-Test-Ban Treaty (CTBT) includes a multipronged approach for monitoring signatory countries for signs of clandestine nuclear testing. If a nuclear detonation is suspected, seismic, infrasound, atmospheric, and satellite data will be used to investigate the event remotely. If enough evidence exists, member countries may vote for an on-site inspection, and sampling for trace radionuclide gases will be performed at or near the surface in the vicinity of the best-guess location of the UNE. The on-site inspection presents the final opportunity to collect data to confirm or deny whether the country is in violation of the treaty, and radionuclide gas detection is one of the best ways to determine if an underground explosion has been nuclear in nature. One of the gases of interest for on-site inspections is  $^{133}\text{Xe}$  (half-life 5.243 d). Because  $^{133}\text{Xe}$  decays rapidly, the window of opportunity for detection is limited. Without an estimate of the gas arrival time and the window of opportunity for detection, the on-site inspection may fail to detect available gases.

For vadose zone UNEs that do not immediately vent detectable concentrations of radionuclides into the atmosphere (i.e., a well-contained test),  $^{133}\text{Xe}$  may still migrate through

the chimney zone and overlying rock and soil to the surface at timescales of weeks to months (Carrigan and Sun, 2014). Gaseous diffusion alone cannot bring  $^{133}\text{Xe}$  to the surface before it has decayed beyond detectability (Carrigan, 1994). However, the upward ratcheting of trace gases along fractures by barometric pumping (Nilson et al., 1991) may transport  $^{133}\text{Xe}$  quickly enough for detection in some instances (Fig. 1). Barometric pumping is a mechanism by which atmospheric pressure variations can drive underground vapor-phase contamination to the surface. It has been observed, for example, at sites where underground solvent disposal has resulted in volatile organic compound (VOC) plumes (Neeper and Stauffer, 2012) and where tracer gases have been explosively introduced deep underground to test the influence of barometric pumping on radionuclide gas transport from underground nuclear weapons tests (Carrigan et al., 1996). The process works by advective transport of gases following transient pressure gradients, while concurrent diffusion, dispersion, and mobile-immobile phase exchange processes serve to “ratchet” the contaminant of interest upward during successive barometric cycles.

Numerical and analytical modeling of gas transport from UNEs in the unsaturated zone was performed by Nilson and Lie (1990) and Nilson et al. (1991), who used double-porosity models to study the effects of oscillatory barometric pumping in a fractured porous material. The theory of soil gas movement under the influence of barometric pumping was explored by Massmann and Farrier (1992), Auer et al. (1996), Scanlon et al. (2001), and Neeper and Stauffer (2012), among others. Carrigan et al. (1996) and Sun and Carrigan (2014) have developed numerical models for vadose zone transport of radionuclide gases from UNEs in fractured rock with

barometric pumping. Double-porosity modeling of subsurface transport of Xe isotopes from UNEs has also been used to show the effects of uncertain geologic properties on the fractionation of various Xe isotopes ( $^{133}\text{Xe}$ , metastable  $^{133}\text{Xe}$  and  $^{131}\text{Xe}$ , and  $^{135}\text{Xe}$ ) (Lowrey et al., 2013).

Gaining insights into the magnitude and form of uncertainties in predicted gas breakthrough as a result of uncertain geologic parameters (fracture aperture, matrix permeability, porosity, and saturation) was the primary objective of this research. The influence of hydrogeologic parameters on gas breakthrough is complex and nonlinear, as demonstrated by the analytical modeling of Nilson et al. (1991) and Auer et al. (1996) and the numerical modeling of Sun and Carrigan (2014). Fracture aperture and matrix permeability are universally recognized as important factors in barometric pumping efficiency. Other geologic factors studied by prior researchers include fracture spacing (Nilson et al., 1991), the rubbilization (permeability and porosity enhancement) of a chimney zone (Jordan et al., 2012), effective gas diffusivity in the porous material (Sun and Carrigan, 2014), and the effect of an alluvium layer of variable permeability (Sun and Carrigan, 2014). Less well characterized were the effects of porosity and saturation, although air-filled porosity is one factor in the bulk pneumatic diffusivity tested by Nilson et al. (1991). Porosity and saturation affect the barometric ratcheting processes through storage, both in terms of filtering gases into the matrix material and Henry’s Law partitioning of soluble gases into the aqueous phase. Both parameters also have complex feedbacks on diffusivity, by way of the tortuosity of the material.

The model developed in this study was used to perform sensitivity analyses to investigate the isolated effects of fracture aperture, matrix permeability, porosity, and saturation and boundary conditions such as atmospheric forcing in different seasons of the year on the barometric ratcheting process. The results of the sensitivity tests and Monte Carlo simulations provided new insights into radionuclide gas transport processes under the influence of barometric pumping in a fractured dual-permeability medium.

In a scenario with many geologic uncertainties, limited site-specific data, and the short turn-around time required to obtain results of use to the international community, the construction of a subsurface model with high fidelity may not be possible. We also used a method where thousands of Monte Carlo simulations were performed across a range of rock properties for a particular rock type and explosion characteristics. The resulting range of  $^{133}\text{Xe}$  breakthrough provides an estimated range for the arrival time and window of opportunity for detection. We validated the model with available gas migration data from the Non-Proliferation Experiment (NPE), a 1.07 kt chemical explosion detonated underground at the Nevada National Security Site (NNSS) on 22 Sept. 1993, with bottles of tracer gases emplaced near the detonation point (Carrigan et al., 1996). The model validated with tracer gas

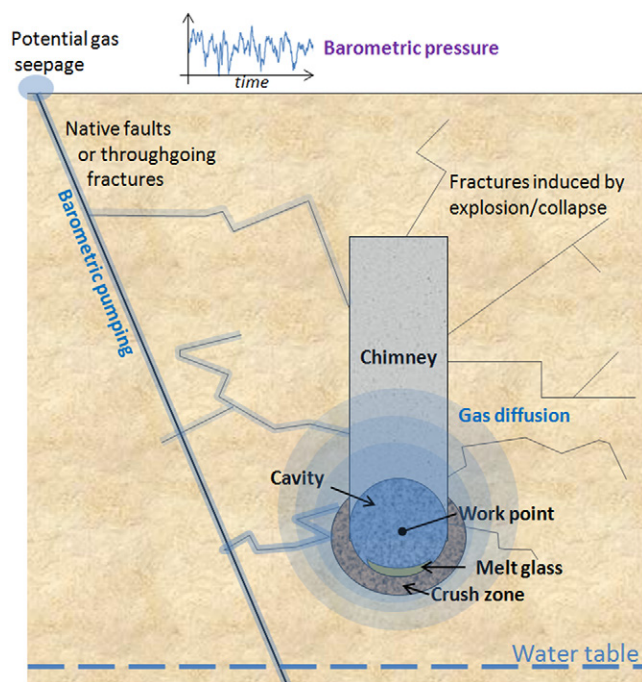


Fig. 1. Conceptual model for gas transport by barometric pumping in the vadose zone following an underground nuclear detonation.

data was compared with a “blind” Monte Carlo prediction of gas breakthrough in which it was assumed that no data were available.

The methods used in this study differ from previous modeling work through our focus on comparing the effects of four particular hydrogeologic parameters (fracture aperture, matrix permeability, porosity, and saturation) and examination of their interrelated impacts in a Monte Carlo study. Our model domain included the explosion cavity and chimney, and extended far enough horizontally to capture lateral gas loss. Finally, the seasonal analysis is new; the cumulative effects of oscillations of varying frequency and amplitude in the barometric signal can play a significant role in the efficiency of the barometric ratcheting process (Nilson et al., 1991; Neeper and Stauffer, 2012), but the effect had not been explored for radionuclide migration in fractured rock in a numerical model with a realistic, seasonally variable pressure signal.

## Numerical Model

### Porous Simulator and Particle Transport

The Finite Element Heat and Mass transfer code (FEHM), a multiphase flow and transport model developed at Los Alamos National Laboratory, was used for all simulations. The control volume finite element method is used in FEHM to find approximate solutions to the governing equations of mass and momentum conservation, assuming that a multiphase form of Darcy’s law is valid for all phases across the domain (Zyvoloski et al., 1997; Zyvoloski, 2007). Multiple studies focusing on vapor transport in the unsaturated zone have used FEHM (e.g., Mihopoulos et al., 2002; Stauffer et al., 2005; Kwicklis et al., 2006; Neeper and Stauffer, 2012). The simulator was benchmarked against a suite of test problems provided by Dash (2003) following all code modifications.

The fracture and surrounding matrix were modeled as a dual-permeability medium (Jordan et al., 2012). Because our focus was on gas flow, we simulated water in the pore spaces as immobile after the initial specification of saturation throughout the domain. In the model, the gases could partition into the aqueous phase, with Henry’s Law coefficients given in Table 1.

The simulations were isothermal, which may be a reasonable assumption for late-time (weeks to months following the detonation) transient gas flow far from the cavity because the noncondensable hot gases equilibrate to the rock temperature quickly due to their much lower total heat capacity (Morrison, 1973). The lack of tracer gas arrival at the surface shortly after the NPE suggests that isothermal models featuring barometric pumping as the primary driving mechanism, such as that of

Carrigan et al. (1996), are acceptable for this case; however, the rock close to the work point of a real UNE (as compared to a chemical explosion) may be significantly hotter for a longer period of time (Tompson et al., 2002), probably providing a stronger initial driving force for distributing gases (Sun and Carrigan, 2014).

It will not be generally known at a particular UNE site whether thermal convection will transport gases quickly to the surface or to considerable distances beyond the cavity and chimney. If the explosion is “well contained,” i.e., no immediate venting of gases, it can only be assumed that thermal processes were not sufficient to transport radionuclide gases all the way to the surface. Because this research considered late-time seepage of gases through considerable overburden in cases where no venting has occurred, residual test heat was neglected.

The tracer gases of the NPE ( $\text{SF}_6$  and  $^3\text{He}$ ) and one radionuclide of interest for UNEs ( $^{133}\text{Xe}$ ) were simulated in FEHM by numerical approximation of the advection–diffusion equation (Fetter, 1999). The numerical scheme was fully implicit and included full upstream weighting of transmissibilities (Zyvoloski et al., 1997). Dispersivity in the matrix was neglected because velocities in the matrix were small ( $\sim 1 \times 10^{-9} \text{ m s}^{-1}$ ) and transport there was diffusion dominated.

For each gas, the effective diffusion coefficient was estimated by multiplying the binary free-air diffusion coefficient by a tortuosity calculated using the Millington–Quirk approach:

$$\tau = \frac{\theta_a^{7/3}}{n^2} \quad [1]$$

where  $\theta_a$  is the air-filled porosity and  $n$  is the total porosity (Millington and Quirk, 1961; Baehr, 1987). The Millington–Quirk model has been found to match experimental data well for solute diffusion in liquid in unsaturated fractured rock (Stauffer et al., 2009). For gases in soils, Jin and Jury (1996) showed that other models may provide a better fit to experimental data, but the effect on our results would be minimal. The free-air molecular diffusion coefficients for  $^3\text{He}$ ,  $\text{SF}_6$ , and  $^{133}\text{Xe}$  are given in Table 1. The effective diffusion coefficients for dissolved gases in pore water were calculated similarly, but are much smaller (Table 1).

Table 1. Transport model parameters.

Parameter	$^3\text{He}$	$\text{SF}_6$	$^{133}\text{Xe}$
Henry’s Law coefficient ( $K_H^\circ$ ), $\text{mol kg}^{-1} \text{ MPa}^{-1}\dagger$	0.00375	0.0024	0.043
Molecular diffusion coefficient in air ( $D_a$ ), $\text{m}^2 \text{ s}^{-1}\ddagger$	$7.6 \times 10^{-5}$	$9.1 \times 10^{-6}$	$1.24 \times 10^{-5}$
Molecular diffusion coefficient in water $D_w$ , $\text{m}^2 \text{ s}^{-1}$	$6.5 \times 10^{-9}\S$	$1.2 \times 10^{-9}\P$	$1.5 \times 10^{-9}\S$

† From Sander (2013).

‡ From Carrigan et al. (1997).

§ From Jähne et al. (1987).

¶ King and Saltzman (1995).

## Model Setup

The two-dimensional Cartesian model domain used for sensitivity analyses and for Monte Carlo simulations consisted of homogeneous porous material intersected by a single vertical fracture (Fig. 2). The numerical mesh had uniform spacing in the  $y$  direction and geometrically increasing element size in the  $x$  direction away from the central fracture. There were 12,600 nodes in the 400-by-400-m model domain. The simulations were run for 500 or 1000 d, with a maximum time step size of 0.1 d. The depth of the explosion and amount of  $^3\text{He}$  and  $\text{SF}_6$  produced were designed for comparison with NPE data.

The single-fracture model was motivated by NPE gas-sampling results that showed gases first arrived at the surface along faults (Carrigan et al., 1996). Fracturing at scales smaller than the primary channel was not represented explicitly. Permeability due to smaller fractures was considered to be lumped with the bulk permeability to air of the undisturbed matrix material and post-explosion chimneys, which in this study covered a range based on air-permeability experiments in the fractured tuffs at Rainier Mesa (Burkhard et al., 1987; Nilson et al., 1991).

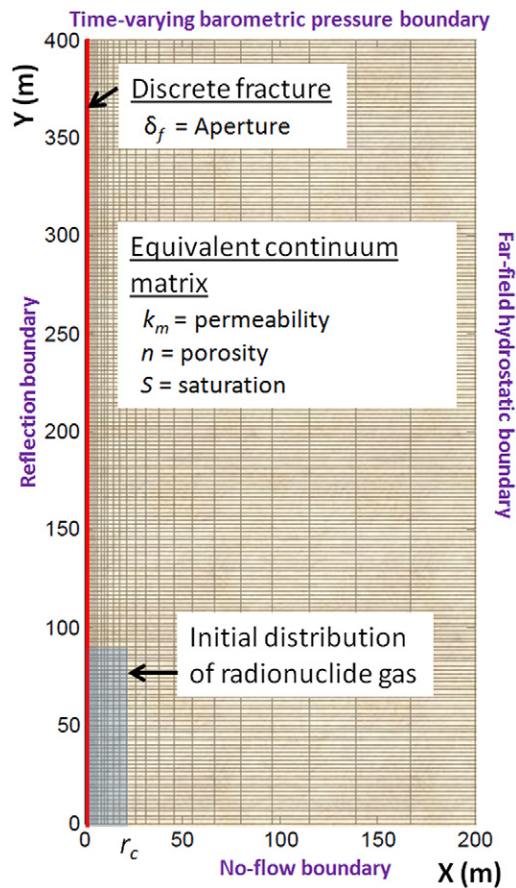


Fig. 2. Two-dimensional grid schematic with fracture and initial gas distribution (shaded region). The actual grid was 400 by 400 m, symmetric about the fracture. The gases were initially distributed at the appropriate concentrations within a region one cavity radius ( $r_c$ ) in width and  $5r_c$  in height.

The boundary conditions at the simulated ground surface were a time-varying barometric pressure signal and uncontaminated fresh air. The barometric pressure data that were collected for 83 d before the NPE (Carrigan et al., 1996) were used to initialize the simulations before turning on tracer transport. Boundary conditions were vapor-static pressures and zero concentration in the far-field limit. Pressures in the cavity and chimney were assumed to have returned to in situ vapor-static conditions following cavity collapse. The bottom of the domain was a no-flow boundary, representing a hypothetical saturated zone below the simulation.

It was assumed that cavity collapse caused a chimney zone, with gases homogeneously mixed within the chimney volume. The NPE tracer gases (57.3 mol  $^3\text{He}$ , 357 mol  $\text{SF}_6$ ) and UNE byproduct  $^{133}\text{Xe}$  ( $7.7 \times 10^{-3}$  mol) (Carrigan et al., 1997) were initially distributed in this chimney zone of width twice the cavity radius ( $r_c$ ) and height  $5r_c$  at concentrations computed by assuming a cylindrical volume. The cavity radius was  $r_c = 16.8$  m (total chimney width = 33.6 m) and  $5r_c = 84$  m for the initial zone of gas contamination for most simulations, based on interpretation of seismic data from Stump et al. (1999). Background concentrations of the gases in the subsurface and atmospheric boundary were assumed to be zero, although  $\text{SF}_6$ ,  $^3\text{He}$ , and  $^{133}\text{Xe}$  all have low background concentrations in air (Carrigan et al., 1996; Geller et al., 1997; Hebel, 2010). Our current work did not address other Xe isotopes or the contribution from  $^{133}\text{Xe}$  precursors (radioiodine) to the original  $^{133}\text{Xe}$  source term (Lowrey et al., 2013).

## Monte Carlo and Sensitivity Methods

The parameter suite for Monte Carlo analysis was generated by Latin hypercube sampling for values of matrix porosity ( $n$ ), matrix permeability ( $k_m$ ), saturation ( $S$ ), and the fracture aperture ( $\delta_f$ ) across the ranges shown in Table 2. A set of 2000 realizations was performed, with these four rock properties allowed to vary among the realizations. The ranges in Table 2 represent a wide span based on geologic investigations at Rainier Mesa (e.g., Thordarson, 1965; Townsend et al., 2007; Ebel and Nimmo, 2012). Fracture apertures were chosen to achieve subsurface air permeabilities within the range suggested in the literature; Nilson et al. (1991) reported bulk pneumatic diffusivities on the order of 0.1 to  $15 \text{ m}^2 \text{ s}^{-1}$  for volcanic rocks at the NNSS, where the bulk pneumatic diffusivity  $\alpha$  is given by

$$\alpha = \frac{k\bar{p}_0}{\mu n} \quad [2]$$

where  $k$  is the bulk permeability of the matrix and fracture material combined,  $\bar{p}_0$  is the mean barometric pressure,  $\mu$  is the viscosity of air, and  $n$  is the matrix porosity. For fracture material in the dual-permeability model, individual fracture permeability ( $k_f$ ) was calculated as  $\delta_f^2/12$  (Witherspoon et al., 1980).

The sensitivity of the numerical model to  $n$ ,  $\log(k_m)$ ,  $S$ , and  $\delta_f$  was examined by selecting a “base case” from the Monte Carlo

simulations that corresponded to a good match to the NPE data and smoothly varying the critical parameters individually around the base case values (Table 2). To test the impact of the season of the underground test on gas arrival, the 1 July 1993 to 30 June 1994 pressure data from the NPE (Carrigan et al., 1996) were transformed into a continual loop with a 1-yr cycle. The NPE was then simulated as taking place on 22 March, 22 June, and 22 December, in addition to the actual date of 22 September, and the simulations were run for 1000 d. During this particular year at Rainier Mesa, the greatest barometric fluctuations occurred between October and May, with an extended period of relatively high and flat barometric pressures in the summer and early fall. The ratio of the variance of pressure from the period 1 November to 23 May (the “stormier” season) to the rest of the year-long cycle (the “calmer” season) was 2.7.

The window of opportunity for  $^{133}\text{Xe}$  detection in all simulations was determined based on a detection limit of  $0.58 \text{ mBq m}^{-3}$  (Dresel and Waichler, 2004). Although concentrations of  $^{133}\text{Xe}$  may drop below the detection limit and then rise above it again due to barometric pressure changes, the window of detectability was assumed to end at the time when  $^{133}\text{Xe}$  was no longer continuously detectable. Therefore, in practice, the effective detection window may be longer than those calculated here.

## Results

The following model analyses are discussed below: (i) local sensitivity studies testing the impact of each varying hydrologic parameter on arrival times and window of opportunity for Xe detection; (ii) simulations with altered barometric pressure forcing, representing detonations in different seasons of the year; and (iii) Monte Carlo suites with random sampling across the parameter space to determine interactions and global sensitivity and to predict  $^{133}\text{Xe}$  detectability for a 1 kt UNE in tuff. Table 2 summarizes the analyses performed and the ranges of variable properties used for these tests. Additional simulations were previously performed to analyze the effects of the initial gas distribution and the presence of a highly rubblized cavity and chimney area (Jordan et al., 2012).

### Sensitivity to Hydrologic Parameters

Figure 3 shows the NPE tracer gas arrival data presented in Carrigan et al. (1996). The arrival of  $\text{SF}_6$  and  $^3\text{He}$  in the simulation (50 and 387 d after the explosion, respectively)

Table 2. Description of analyses performed and ranges of parameters used for this study.

Simulations	Factor	Porosity	Saturation	Matrix permeability	Fracture aperture
no.				$\text{m}^2$	mm
Sensitivity analysis†					
100 for each parameter (400 total)	base case	0.29	0.3	$9.1 \times 10^{-15}$	1.5
	range	0.1–0.36	0.01–0.5	$1 \times 10^{-16}$ – $1 \times 10^{-13}$	0.8–3
Seasonal sensitivity analysis†					
100 for each parameter for four seasons (1600 total)	base case	0.29	0.3	$9.1 \times 10^{-15}$	1.5
	range	0.1–0.36	0.01–0.5	$1 \times 10^{-16}$ – $1 \times 10^{-13}$	0.8–3
Monte Carlo analysis‡					
2000	range	0.1–0.36	0.01–0.5	$1 \times 10^{-16}$ – $1 \times 10^{-13}$	0.8–3

† Parameters uniformly varied.

‡ Latin Hypercube sampling of varying parameters.

corresponds well with the experimental data of Carrigan et al. (1996):  $\text{SF}_6$  arrival 49 d after the explosion,  $^3\text{He}$  after 379 d.

Figure 4 shows normalized concentrations of the two tracer gases at the top of the fracture (land surface), at various times, for each of the four parameters that varied. Because the barometric pressure at the surface at a given time controls the absolute concentration at the top of the fracture, variations about the mean value are shown for three times. The sensitivity of concentration at the surface to the input parameters tended to decrease slightly with time. At extremely low concentrations, which applied mostly to  $^3\text{He}$  at early times, the numerical model failed to show sensitivity to saturation, matrix permeability, or fracture aperture.

The direct relationship between gas concentration at the surface and water saturation, and the inverse relationship between

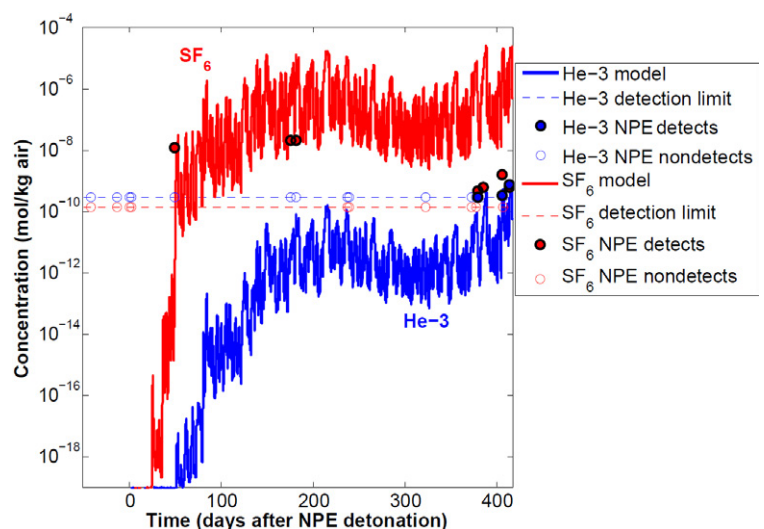


Fig. 3. Base case simulated breakthrough curves from the numerical model at the top of the fracture (land surface) for  $^3\text{He}$  and  $\text{SF}_6$ . Non-Proliferation Experiment (NPE) data are shown as open circles (nondetects) and filled circles (detections). Dashed lines are the NPE detection limits for  $^3\text{He}$  and  $\text{SF}_6$ .

gas concentration and porosity, are both indications of the amount of air-filled porosity ( $\theta_a$ ) having an inverse relationship with the facility of gas transport to the surface. To first order, this result is caused by decreased storage for gas and hence faster travel times. (At high saturations, however, gas permeabilities are dampened due to multiphase effects.) Additionally, the relationship between porosity, air-filled porosity, and tortuosity is given in Eq. [1], where factors causing an increase in the tortuosity coefficient  $\tau$  increase the effective diffusion coefficient, and greater diffusivity leads to lower concentrations available to transport up the fracture during barometric low cycles (as seen by the differences between  $^3\text{He}$  and  $\text{SF}_6$ , gases of very different diffusivity).

Figure 4 also shows that the heavier, less diffusive gas ( $\text{SF}_6$ ) is less sensitive to the parameters than the lighter  $^3\text{He}$ . For matrix permeability and fracture aperture, there is a logarithmic relationship with concentration, indicating extreme sensitivity in part of the range and very little sensitivity in the rest of the range.

Arrival times for  $\text{SF}_6$ ,  $^3\text{He}$ , and  $^{133}\text{Xe}$  for the sensitivity simulations are shown in Fig. 5. The date of first gas detection, which is of particular interest in the context of on-site inspection, does not vary smoothly like concentration because weather events cause sharp changes in concentration at the surface and tracer gases for many simulations will cross the detection threshold at once. Thus there are discrete batches of simulations where gases break through at the same time.

The arrival time of  $^3\text{He}$  is more sensitive to the varied parameters than  $\text{SF}_6$  and  $^{133}\text{Xe}$ . Within the ranges selected for the parameters (Table 2), only fracture aperture has an extreme effect on  $\text{SF}_6$  arrival time, with very small fracture apertures delaying the first arrival of gas to around 2.5 yr. Arrival times for  $^{133}\text{Xe}$  are capped by the difficulty that the gas decays to nondetectability if the gas is delayed while traveling to the surface. Although  $^{133}\text{Xe}$  has a diffusivity between that of  $^3\text{He}$  and  $\text{SF}_6$  (Table 1), it has a significantly lower practical detection limit than those used in the mid-90s for the tracer gases of the NPE, and hence arrival times are slightly earlier than those of  $\text{SF}_6$ . This result provides crucial information for quantifying the effect of uncertainties in hydraulic parameters on  $^{133}\text{Xe}$  breakthrough at the surface for collection in an on-site inspection. Arrival times for Xe ranged from 15.8 to 84 d following the detonation, with some cases with very small matrix permeability ( $<2.1 \times 10^{-15} \text{ m}^2$ ) and fracture aperture ( $<1.1 \text{ mm}$ ) resulting in no breakthrough at all.

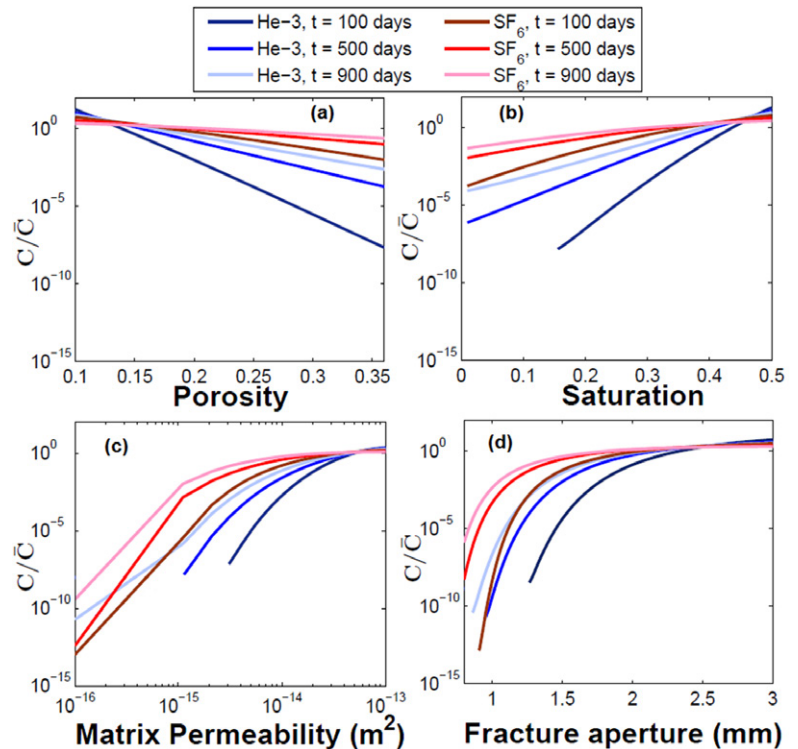


Fig. 4. Relative concentration ( $C/\bar{C}$ ) of  $^3\text{He}$  and  $\text{SF}_6$  at the top of the fracture at three different times ( $t = 100, 500$ , and  $900$  d following the Non-Proliferation Experiment detonation) for varying (a) saturation, (b) porosity, (c) matrix permeability, and (d) fracture aperture. Mean concentration  $\bar{C}$  is calculated at each time shown for each parameter varied.

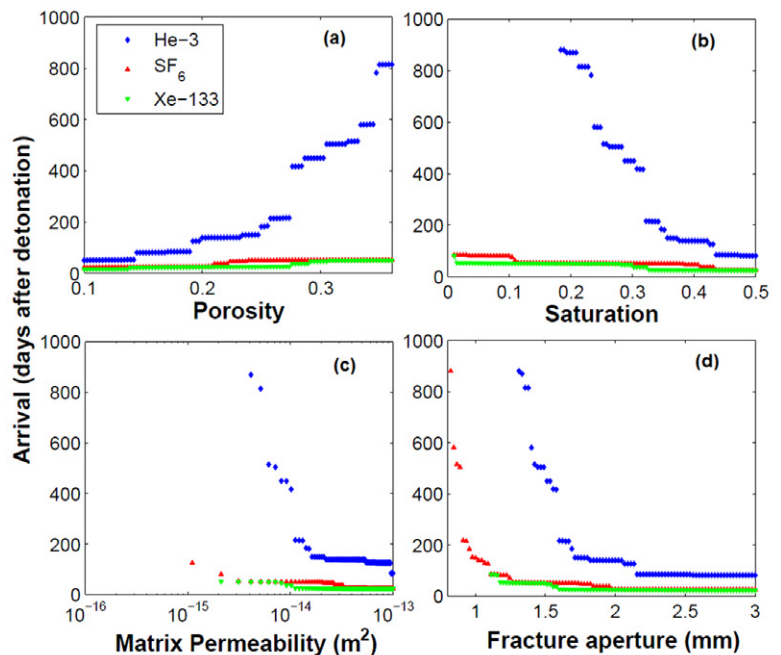


Fig. 5. Arrival time for  $^3\text{He}$ ,  $\text{SF}_6$ , and  $^{133}\text{Xe}$  with varying rock parameters: (a) porosity, (b) saturation, (c) matrix permeability, and (d) fracture aperture. For each parameter, 100 simulations uniformly spanned the range of possible values. Due to radioactive decay of  $^{133}\text{Xe}$ , if gas transport was not rapid enough, arrival did not occur. Note that although the diffusivity of  $^{133}\text{Xe}$  falls between  $^3\text{He}$  and  $\text{SF}_6$  (Table 1), arrival times were earlier for  $^{133}\text{Xe}$  because its detection limit is lower.

The length of the detection window for  $^{133}\text{Xe}$  is shown in Fig. 6. The window is quite sensitive to all parameters, with the chosen ranges of parameters creating windows as small as 0 d and as large as 136 d. As the arrival time grows longer, the window of opportunity shrinks due to radioactive decay; therefore, any parameter change that results in quicker gas arrival also generally produces a longer window of opportunity for detection. However, the behavior is non-monotonic.

## Seasonal Effects

The effect of the season of detonation on the arrival time of  $^{133}\text{Xe}$  across the ranges of parameters used in the sensitivity studies (Table 2) is shown in Fig. 7. The results show that, given the conditions and assumptions of the numerical model, a detonation in March is the least likely to produce detectable  $^{133}\text{Xe}$  for the location (Rainier Mesa) and particular year of pressure history used. In general, a greater degree of barometric variability results in quicker gas transport to the surface, but we show here that the effect is dependent on subsurface hydrologic properties. For example, with a small fracture aperture (Fig. 7d), detonations in March take so long to move  $^{133}\text{Xe}$  toward the surface that it decays below the detection threshold, while with a large fracture aperture, detonations in June and September arrive slightly later than detonations in March.

The window of opportunity for  $^{133}\text{Xe}$  detection is shown in Fig. 8. For this UNE scenario at Rainier Mesa, for this year of pressure data, March detonations had the smallest window of detectability, while December detonations had the longest windows of opportunity for  $^{133}\text{Xe}$  detection.

The effects of seasonal differences in barometric pressure on radionuclide gas arrival will obviously be site specific. For sites with strong divergence between the summer and winter weather, the season of detonation may make a significant difference in the likelihood of event detection. The transport efficiency for sinusoidally oscillating flow was discussed by Nilson et al. (1991), who found a maximum efficiency when the period of oscillation and the timescale for diffusion between the contaminated air and fresh air were comparable. That is, for a very high-frequency barometric cycle, only a small layer of contaminated porous material adjacent to the fracture can contribute to the contaminated air in the fracture, while for a very low-frequency cycle, the net transport of gas to the surface per cycle is limited by the nearly complete return of contaminated air into the large storage volume adjacent to the fracture in the initially uncontaminated space. Reduction of the amplitude of pressure variation also reduces the barometric pumping efficiency by decreasing the gas penetration depth (Nilson et al., 1991).

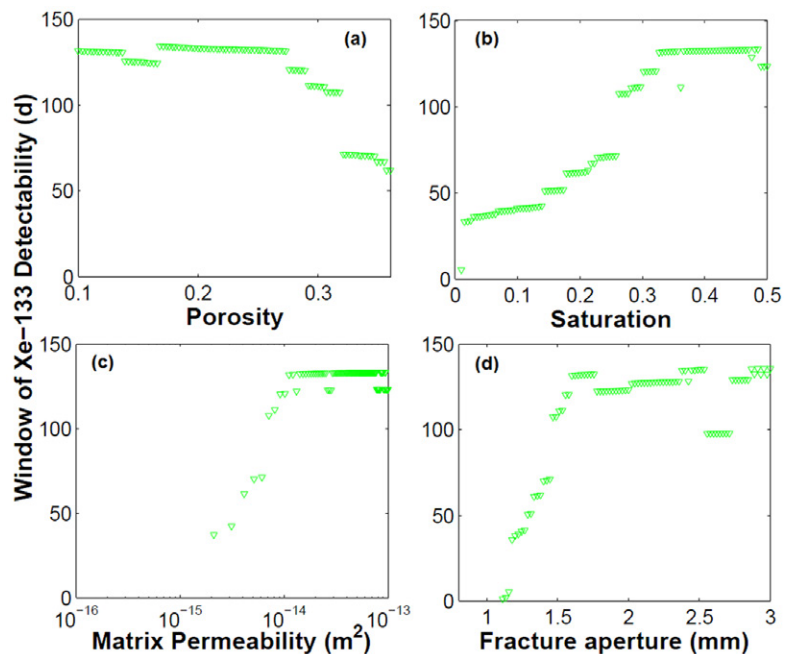


Fig. 6. Window of opportunity for detection of  $^{133}\text{Xe}$  with varying rock parameters: (a) porosity, (b) saturation, (c) matrix permeability, and (d) fracture aperture.

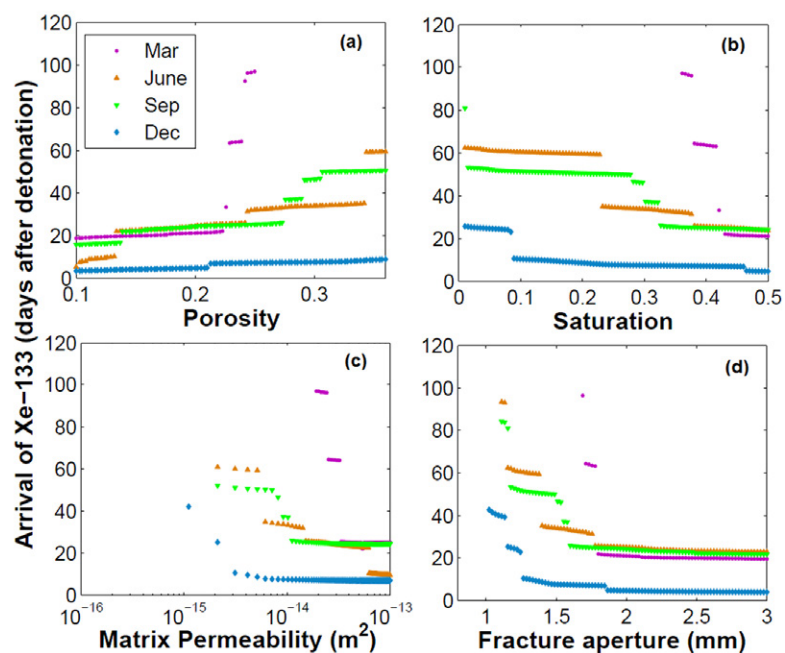


Fig. 7. Arrival time for  $^{133}\text{Xe}$  with varying season of detonation and rock parameters: (a) porosity, (b) saturation, (c) matrix permeability, and (d) fracture aperture. The length of all simulations was 500 d.

## Monte Carlo Simulations

The Monte Carlo simulations were used to test the coupled effects from simultaneously varying fracture and matrix parameters on tracer gas and  $^{133}\text{Xe}$  arrival times. Sensitivity analysis was performed using PSUADE to rank the sensitivity of  $^3\text{He}$  and  $\text{SF}_6$  arrival times to the varied input parameters (Tong, 2005). The difference in sensitivities of the two gases of varying diffusivity is

illustrative of the complexity of the barometric ratcheting process in a fractured porous material. The methods used in PSUADE to rank sensitivity to parameters included the Spearman rank correlation coefficient, standard regression coefficient (linear), MARS sensitivity score, sum-of-trees sensitivity score, delta test sensitivity score, and Sobol' first-order index (Tong, 2005; Gan et al., 2014). As is commonly seen in highly nonlinear hydrologic applications, the rankings varied according to the method used, and we elected to eliminate the Spearman and standard regression coefficient rankings (e.g., Gan et al., 2014). For  $^3\text{He}$  arrival time, the remaining methods agreed on permeability as the most sensitive parameter, with fracture aperture and saturation tying for the second most sensitive parameter, and porosity generally as the least sensitive. For  $\text{SF}_6$  arrival time, all methods indicated fracture aperture as the most sensitive parameter, with permeability always ranked second, and porosity and saturation tying for least sensitive.

In fewer than half of the simulations (758, 38%), both tracer gases ( $^3\text{He}$  and  $\text{SF}_6$ ) broke through at the surface by 500 d. Sulfur hexafluoride always arrived before  $^3\text{He}$ , but many realizations did not show the spacing of nearly 11 mo between  $^3\text{He}$  and  $\text{SF}_6$  arrival observed during the NPE (Fig. 9). In many cases,  $^3\text{He}$  arrived during earlier barometric lows than observed, whereas  $\text{SF}_6$  typically arrived anywhere from early to on-time relative to the NPE data.

The arrival times of gases were clustered around specific weather events that produced barometric low pressures. The significant barometric low pressure event beginning  $\sim 49$  d after the NPE detonation (10 Nov. 1993) produced  $\text{SF}_6$  and  $^3\text{He}$  breakthrough in many of the Monte Carlo simulations. However, in the experimental data,  $^3\text{He}$  did not break through at this time but much later during a barometric low pressure event in October 1994 after the relatively quiescent summer and early fall months (Fig. 9).

Further comparisons were made between the subsets of realizations that (i) achieved breakthrough in 500 d and (ii) matched the NPE data. Figure 10 shows histograms of the number of realizations with various porosities, saturations, permeabilities, and fracture apertures that met those criteria. From the uniform random samples

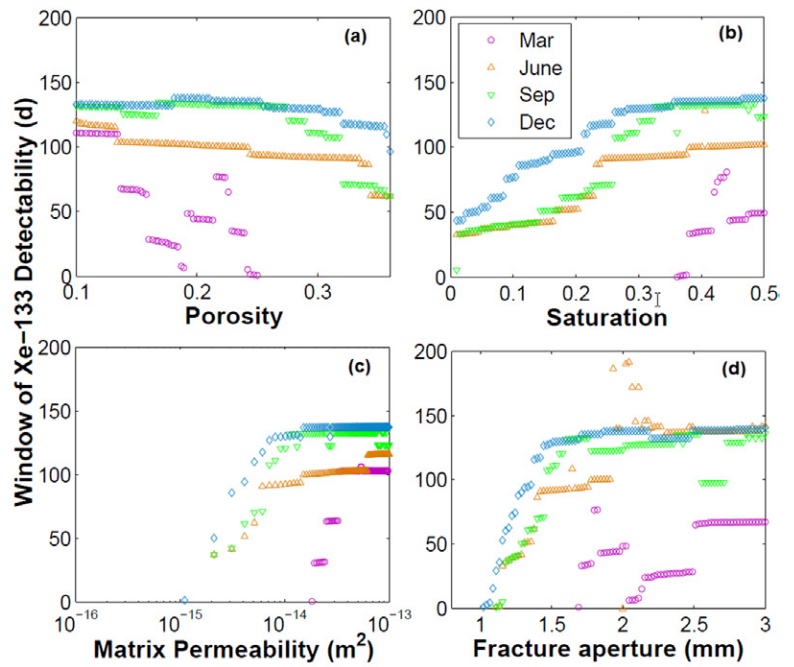


Fig. 8. Window of opportunity for  $^{133}\text{Xe}$  with varying season of detonation and rock parameters: (a) porosity, (b) saturation, (c) matrix permeability, and (d) fracture aperture.

across the parameter space (green), the simulations most likely to have gas breakthrough in the time of the simulation (blue) were the ones with lower air-filled porosity (smaller porosity, greater saturation) and higher permeabilities (matrix and fracture). However,

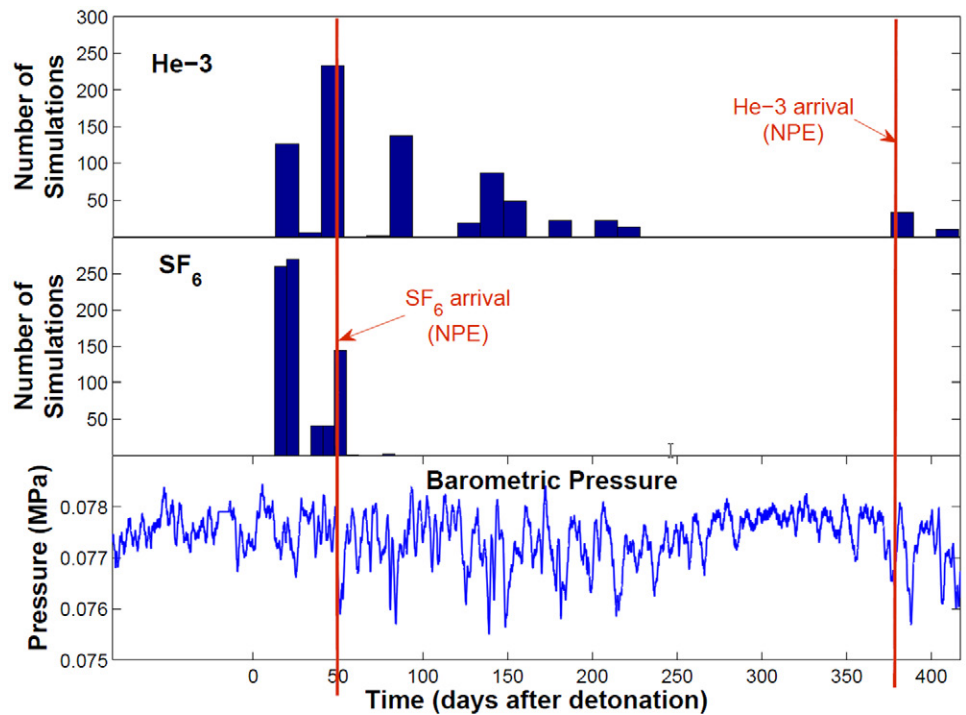


Fig. 9. Arrival time histograms for  $^3\text{He}$  and  $\text{SF}_6$ . Gas arrivals correspond to low barometric pressure weather events. Actual arrival of  $^3\text{He}$  and  $\text{SF}_6$  during the Non-Proliferation Experiment (NPE) are shown. Pressure data are from Carrigan et al. (1996).

beyond a certain fracture aperture ( $\sim 2$  mm), fracture aperture did not appear to matter anymore. Realizations matching the NPE data (red) had properties spanning essentially the entire ranges of the chosen parameter space.

Although the original input data were uncorrelated (Latin Hypercube sampling), among the simulations where breakthrough occurred in the range of time observed at the NPE,  $S$  was negatively correlated with matrix permeability and fracture aperture, while porosity was directly correlated with matrix permeability and fracture aperture. In both cases, this implies that for a higher air-filled porosity  $\theta_a = n(1 - S)$ , higher permeabilities (both matrix and fracture) were required to transport the tracer gases to the surface during the time frame of the observed NPE gas arrival.

The *difference* in breakthrough arrival time for  $^3\text{He}$  and  $\text{SF}_6$  (number of days after  $\text{SF}_6$  arrival until  $^3\text{He}$  breakthrough) was negatively correlated with  $S$  and positively correlated with  $n$ , and negatively correlated with matrix permeability and fracture aperture. This implies that each of the input parameter changes that delays arrival time, as seen in the sensitivity studies above, leads to increased delays for  $^3\text{He}$  relative to  $\text{SF}_6$  arrival; that is, any change that results in longer travel time for the gases leads to greater “chromatographic” separation between the two gases of different weights.

The arrival of the tracer gases with the observed separation was also correlated with the ratio of fracture aperture to matrix permeability ( $p = 0.017$ ) and the ratio of air-filled porosity to matrix permeability ( $p = 0.016$ ) while being uncorrelated with any individual parameter. This observation suggests the interrelationships required to preserve the observed tracer gas separation in arrival time (which cannot be determined solely from the sensitivity of the arrival time of each tracer gas to individual parameters).

The Monte Carlo simulations were also used to demonstrate a method to provide a quick estimate of  $^{133}\text{Xe}$  arrival for a 1 kt UNE in tuff in a geologically simple model, representing a site with extremely limited available data. The “best case” realizations from the Monte Carlo suite were the 32 out of 2000 simulations where both  $^3\text{He}$  and  $\text{SF}_6$  arrived during the same barometric lows as they did during sample collection at the NPE (Fig. 9). For these simulations that closely matched the NPE arrival data, 30 out of 32 (94%) resulted in a window of time where  $^{133}\text{Xe}$  would also theoretically be detectable, with arrival times ranging from 13 to 51 d following the explosion (Fig. 11). The window of detectability for the simulations with  $^{133}\text{Xe}$  breakthrough ranged from 38 to 135 d.

For each day between the first detection and the disappearance of  $^{133}\text{Xe}$ , the percentage of simulations that would produce detections on those days is plotted in Fig. 11b. The CTBT restricts the duration of any on-site inspection to a maximum of 60 d, with possible extension by 70 d (Comprehensive Test Ban Treaty Organization, 2013). If the on-site inspection following the UNE is assumed to

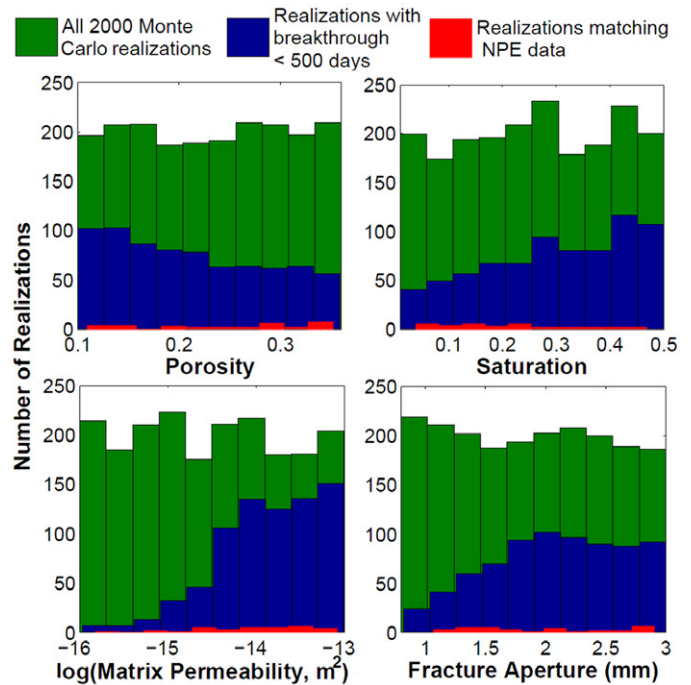


Fig. 10. Histograms of the number of realizations with parameters falling into the chosen ranges of porosity, saturation, matrix permeability, and fracture aperture. Subsets of the full set of realizations corresponding to simulations with both gases arriving by 500 d and simulations with gas arrival matching the Non-Proliferation Experiment (NPE) data are shown.

last just 60 d, the most probable 60-d window for gas detection should be selected.

In a realistic scenario involving a site with uncertain geologic properties and no prior “tracer gas” experiments, however, the full suite of Monte Carlo simulations would be used to predict the  $^{133}\text{Xe}$  arrival time and detection window. Figure 12 shows breakthrough curves for all 2000 simulations and the corresponding percentage of simulations with detectable  $^{133}\text{Xe}$  per day. The “blind” Monte Carlo simulation suite produces a lower percentage of realizations with detectable  $^{133}\text{Xe}$  (61%), with a slight shift in the distribution toward earlier arrival times.

## Discussion

The estimates of the  $^{133}\text{Xe}$  arrival time and window of opportunity presented here provide an approximation for when an on-site inspection team would be most likely to record detections for an UNE with the same basic properties as the NPE (i.e., 1 kt at 389 m below the ground surface in tuff, with evidence of some form of barometric connection to the surface via fault or fracture) but with highly uncertain subsurface properties, including effective gas diffusivity. These values compare well with the NPE model of Carrigan et al. (1996), who predicted  $^{133}\text{Xe}$  arrival 50 d following detonation for an NPE-like UNE, along with a window of opportunity of 85 d (Carrigan and Sun, 2014). The latter study included variations in different

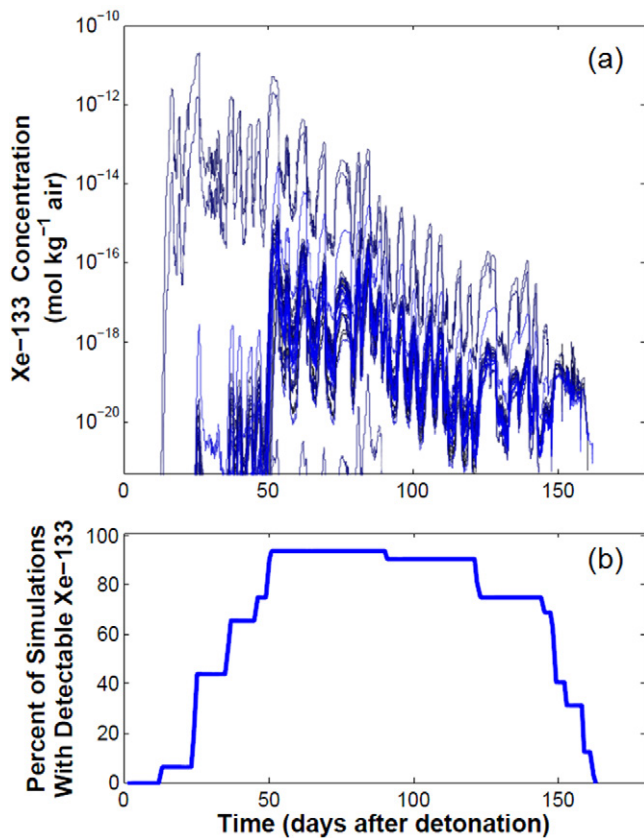


Fig. 11. (a) Breakthrough curves for  $^{133}\text{Xe}$  at the top of the fracture for 32 of the 2000 realizations with tracer gas arrival times matching with the Non-Proliferation Experiment data (“best cases”), where the bottom of the graph corresponds to a detection limit of  $0.58 \text{ mBq m}^{-3}$ ; and (b) the probability of  $^{133}\text{Xe}$  detection for 180 d following detonation of a 1 kt underground nuclear explosion buried 389 m below the ground surface in tuff at Rainier Mesa, based on simulations matching the experiment data.

properties, such as gas diffusivity and overlying soil alluvium permeability. At an unknown site, where gas migration data are not available (as in the case of the NPE at the NNSS with  $^3\text{He}$  and  $\text{SF}_6$ ), the prediction of a window of opportunity for detection will carry wide uncertainty, but even with gas migration data the problem is non-unique enough that a wide span of hydrologic parameters provides a good match to the data (Fig. 10). The resulting impact on  $^{133}\text{Xe}$  prediction is that the arrival time spans a rather large range (13–51 d) (Fig. 11). It is not necessarily an intuitive result that for simulations matching tracer gas data to within a few days for  $^3\text{He}$  and  $\text{SF}_6$ ,  $^{133}\text{Xe}$ , whose diffusivity falls between the two, should show such a wide spread in arrival times. It highlights the complexity of the barometric ratcheting process and the strong impact of geologic uncertainty on the predicted arrival time. Finally, the “blind” Monte Carlo results show an even greater range of  $^{133}\text{Xe}$  arrival, as expected, but the peak probability for detection is only slightly shifted from the data-matched set (Fig. 12b).

Many factors make the prediction of radionuclide gas detectability following an UNE extremely difficult. In the context of on-site

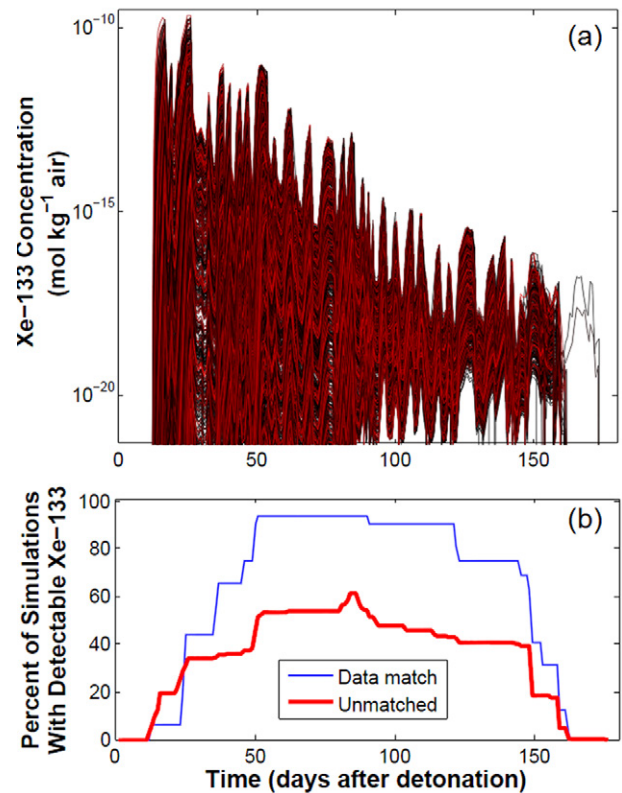


Fig. 12. (a) Breakthrough curves for  $^{133}\text{Xe}$  at the top of the fracture for all realizations, where the bottom of the graph corresponds to a detection limit of  $0.58 \text{ mBq m}^{-3}$ ; and (b) the probability of  $^{133}\text{Xe}$  detection for 180 d following detonation of a 1 kt underground nuclear explosion buried 389 m below the ground surface in tuff for the cases that match the Non-Proliferation Experiment data and for all realizations.

inspection of a country signatory to the CTBT, estimates will need to be provided quickly and potentially without much local subsurface geologic information, requiring simple models—such as the Monte Carlo method presented here—that are fast to produce and run. These models can provide best-guess probabilities, despite great uncertainties, for when to monitor for particular gases, as well as quantitative bounds on the confidence in the prediction. The correlations discussed above, as validated by NPE data, suggest the necessary combinations of parameters (e.g., fracture aperture and matrix porosity) required to produce late-time gas detections via barometric pumping in a fractured, porous material at other potential UNE sites. For detonations in other parts of the world, an analysis of the seasonality of local barometric pressure cycles will be required to determine whether there are adverse conditions for gas transport to the surface by this mechanism.

The initial distribution of radionuclide gases is an important model input and one that is not well known for UNEs, especially considering the effects of rock type, thermal convection, and local hydrogeologic conditions on gas transport in the seconds following the explosion and before ground motion ceases. Comparisons have been made to the NPE tracer gas arrival data to constrain the height of the initial gas distribution: if the region was too short,

$^3\text{He}$  did not arrive in time; if the initial gas region was too tall, the two gases did not achieve the observed separation in arrival times after detonation (49 d for  $\text{SF}_6$ , 379 d for  $^3\text{He}$ ) (Jordan et al., 2012). The difference in the arrival time of two gases of different diffusivities was heightened by any factor that increased the travel time, including the length of “fresh air” space above the initial contaminated zone and the concentration of the gases around the fracture. These results underscore the importance of recognizing the initial gas configuration as a source of significant uncertainty.

In addition to the potential lack of adequate subsurface geologic information, including the subsurface explosion-induced fracture network, complicating factors for predicting gas migration from UNEs in a clandestine setting may also include incomplete knowledge of engineered structures in the subsurface that could provide preferential pathways for gas flow or for barometric connection; uncertainty in estimates of the depth of burial, yield, and geographic location of the detonation from seismic data; and thick soil or alluvium cover that dampens the barometric pressure signal (Sun and Carrigan, 2014). Issues and challenges associated with on-site inspection from an operational perspective were discussed by Carrigan and Sun (2014).

The sensitivity analyses, Monte Carlo simulations of late-time seepage, and the results on the impact of seasonal effects in the barometric signal have relevance to studies of volatile contaminant transport from underground sources in fractured material with a barometric connection to the surface. Examples include passive soil vapor extraction (Neeper and Stauffer, 2012),  $\text{CH}_4$  and VOC leakage from subsurface hazardous waste disposal (Wyatt et al., 1995; Stauffer et al., 2005), leakage from underground petroleum contamination (Pirkle et al., 1992) and  $\text{CO}_2$  sequestration (Oldenburg and Unger, 2003), radon transport in fractured rock (Schery et al., 1982), and barometric pumping around nuclear waste disposal sites such as Yucca Mountain (Ahlers et al., 1999) and the Waste Isolation Pilot Plant. While these applications vary in terms of the nature of the contaminant signal (pulse or step function vs. steady state), the cause of the barometric connection (natural or man-made), and timescales of interest (weeks to years), our sensitivity studies and approach to seasonal analysis are relevant and provide applicable information about the relative importance of uncertain parameters.

Future work will expand these results into three-dimensional and non-isothermal scenarios, as well as incorporate more realistic fracture networks for specific rock types. The focus will remain on understanding the effects of uncertainties on the estimates of gas arrival time and predicting gas migration in a context with little available geologic site data.

## Conclusions

Predicting the window of opportunity for the detection of radionuclide gas seepage from UNEs is of great importance for the

enforcement of the CTBT. To efficiently deploy personnel and equipment for an on-site inspection, the time frame of possible gas detection must be estimated, despite great uncertainties in subsurface geologic properties and extent of fracturing, initial distribution of gases following the UNE, and explosion-altered zones. We conducted numerical analyses of radionuclide gas transport through the unsaturated zone with the aims of understanding of the relative importance of unknown geologic parameters on the arrival time frame of trace gases at the surface and showing the impact of the season of detonation on gas detectability. Furthermore, we predicted an approximate window of opportunity for the detection of  $^{133}\text{Xe}$  from an NPE-like UNE with highly uncertain rock parameters. The results of this work will be used to refine prediction capabilities for the detection of gases from suspected UNEs.

The sensitivity studies across a wide range of parameters showed how each parameter individually affects the arrival time and window of opportunity for the detection of tracer gases ( $\text{SF}_6$  and  $^3\text{He}$ ) and  $^{133}\text{Xe}$ . Across the chosen ranges of parameters, gas arrival time was most strongly affected by matrix permeability and fracture aperture, although saturation and porosity also have important feedbacks in the complex barometric pumping process. The implication is that predictions of gas arrival time will be more uncertain when these parameters are poorly constrained compared with the others studied. Gases having higher diffusivity were more sensitive to uncertainty in the rock properties, and any trend leading to increased arrival time also tended to increase the chromatographic separation between the lighter and heavier gases. While these sensitivity results were tested for a scenario with a particular depth of burial (400 m) and with ranges of rock properties based on tuff at Rainier Mesa, some generalizations may still be drawn from the results, as rock properties vary in every geologic medium (across different ranges). The direction and sense of the sensitivities are not expected to change for materials with similar properties overall, although barometric pumping operating in a very different regime (e.g., a fractured granite with extremely low matrix porosity and permeability) will feature very different results.

The sensitivity studies were first presented based on a detonation in September with Rainier Mesa data (stormy in the fall and winter, quiescent in the spring and summer) and then reproduced for detonations in different seasons. These simulations with the barometric pressure data set on a yearly loop indicated that detonations in March are the least likely to be detectable, due to smaller variations in barometric pressure through the summer months (early July–early September) on Rainier Mesa in 1993 and 1994. The effect depends slightly on the subsurface hydrologic properties. While generalizations may be inferred from these results to other geographic regions with different barometric pressure tendencies, it should be cautioned that these results are specific to the location and weather patterns of the year of data used in this study. Future work will analyze the effect of seasonality (cumulative effect of

barometric cycle frequency, amplitude, and stationarity on gas distribution) in more general cases.

Monte Carlo realizations were performed with parameters uniformly varying across the ranges used in the sensitivity studies. With simultaneously varying parameters, it was observed that the parameters could span essentially the whole range and still have breakthrough in <500 d, depending on the other parameters; however, certain ranges (e.g., extremely low matrix permeability) were much less likely. Of the 2000 realizations, 758 produced gas arrival within 500 d and 32 produced breakthrough of  $^3\text{He}$  and  $\text{SF}_6$  that provided a good match to the NPE data. For simulations matching the NPE data, the arrival of  $^{133}\text{Xe}$  was estimated at 13 to 51 d following detonation, and the window of opportunity, if detectable, ranged from 38 to 135 d. Without matching the NPE data, the “blind” Monte Carlo approach estimated arrival times ranging from 12 to 84 d, with a potential detection window from 1 to 160 d. These breakthrough time estimates are specific to an NPE-like UNE (1 kt, 400-m depth of burial) with a detonation in September following barometric pressure data from Rainier Mesa, 1993–1994, but the method may be readily applied to other scenarios in the event of a clandestine nuclear test.

## Acknowledgments

This research was funded by the Defense Threat Reduction Agency (DTRA) under Award no. DTRA1-11-45391/BRCALL08-Per5-I-2-0008. We would like to thank three anonymous reviewers, whose comments greatly improved this paper. We would also like to thank Ed Kwicklis, Dan Levitt, and Terry Miller of Los Alamos National Laboratory (LANL) for information about Rainier Mesa and its geology; Charles Carrigan and Yunwei Sun of Lawrence Livermore National Laboratory for NPE information and data; and Chris Bradley of LANL for conversations and references related to fracturing caused by UNEs.

## References

- Ahlers, C.F., S. Finsterle, and G.S. Bodvarsson. 1999. Characterization and prediction of subsurface pneumatic response at Yucca Mountain, Nevada. *J. Contam. Hydrol.* 38:47–68. doi:10.1016/S0169-7722(99)00011-X
- Auer, L.H., N.D. Rosenberg, K.H. Birdsell, and E.M. Whitney. 1996. The effects of barometric pumping on contaminant transport. *J. Contam. Hydrol.* 24:145–166. doi:10.1016/S0169-7722(96)00010-1
- Baehr, A.L. 1987. Selective transport of hydrocarbons in the unsaturated zone due to aqueous and vapor phase partitioning. *Water Resour. Res.* 23:1926–1938. doi:10.1029/WR023101p01926
- Burkhard, N.R., J.R. Hearst, and J.M. Hanson. 1987. Estimation of the bulk diffusivity of chimneys using post-shot holes. In: Proceedings of the 4th Symposium on Containment of Underground Nuclear Explosions, Colorado Springs, CO. 21–24 Sept. 1987. Sandia Natl. Lab., Albuquerque, NM, p. 288–315.
- Carrigan, C.R. 1994. The Non-Proliferation Experiment and gas sampling as an on-site inspection activity: A progress report. In: M.D. Denny and S.P. Stull, editors, Proceedings of the Symposium on the Non-Proliferation Experiment (NPE): Results and Implications for Test Ban Treaties, Rockville, MD. 19–21 Apr. 1994. Lawrence Livermore Natl. Lab., Livermore, CA, p. 8–51–8–62.
- Carrigan, C.R., R.A. Heinle, G.B. Hudson, J.J. Nitao, and J.J. Zucca. 1996. Trace gas emissions on geological faults as indicators of underground nuclear testing. *Nature* 382:528–531. doi:10.1038/382528a0
- Carrigan, C.R., R.A. Heinle, G.B. Hudson, J.J. Nitao, and J.J. Zucca. 1997. Barometric gas transport along faults and its application to nuclear test-ban monitoring. Rep. UCRL-JC-127585. Lawrence Livermore National Lab., Livermore, CA.
- Carrigan, C.R., and Y. Sun. 2014. Detection of noble gas radionuclides from an underground nuclear explosion during a CTBT on-site inspection. *Pure Appl. Geophys.* 171:717–734. doi:10.1007/s00024-012-0563-8
- Comprehensive Test Ban Treaty Organization. 2013. Comprehensive Nuclear-Test-Ban Treaty. CTBTO Preparatory Commis., Vienna. [http://www.ctbto.org/fileadmin/content/treaty/treaty\\_text.pdf](http://www.ctbto.org/fileadmin/content/treaty/treaty_text.pdf) (accessed 19 July 2013).
- Dash, Z.V. 2003. Validation test plan for the FEHM application. Version 2.21. Rep. 10086-VTP-2.20-00. Los Alamos National Lab., Los Alamos, NM. [https://fehm.lanl.gov/pdfs/fehm\\_vvp.pdf](https://fehm.lanl.gov/pdfs/fehm_vvp.pdf) (accessed 3 June 2013).
- Dresel, P.E., and S.R. Waichler. 2004. Evaluation of xenon gas detection as a means for identifying buried transuranic waste at the Radioactive Waste Management Complex, Idaho National Environmental and Engineering Laboratory. Rep. PNNL-14617. Pacific Northwest National Lab., Richland, WA.
- Ebel, B.A., and J.R. Nimmo. 2012. An alternative process model of preferential contaminant travel times in the unsaturated zone: Application to Rainier Mesa and Shoshone Mountain, Nevada. *Environ. Model. Assess.* 18:345–363. doi:10.1007/s10666-012-9349-8
- Fetter, C.W. 1999. Contaminant hydrogeology. 2nd ed. Prentice Hall, Upper Saddle River, NJ.
- Gan, Y., Q. Duan, W. Gong, C. Tong, Y. Sun, W. Chu, et al. 2014. A comprehensive evaluation of various sensitivity analysis methods: A case study with a hydrological model. *Environ. Model. Softw.* 51:269–285. doi:10.1016/j.envsoft.2013.09.031
- Geller, L.S., J.W. Elkins, J.M. Lobert, A.D. Clarke, D.F. Hurst, J.H. Butler, and R.C. Myers. 1997. Tropospheric  $\text{SF}_6$ : Observed latitudinal distribution and trends, derived emissions and interhemispheric exchange time. *Geophys. Res. Lett.* 24:675–678. doi:10.1029/97GL00523
- Hebel, S. 2010. Genesis and equilibrium of natural lithospheric radon and its influence on subsurface noble gas samples for CTBT on-site inspections. *Pure Appl. Geophys.* 167:463–470. doi:10.1007/s00024-009-0037-9
- Jähne, B., G. Heinz, and W. Dietrich. 1987. Measurement of the diffusion coefficients of sparingly soluble gases in water. *J. Geophys. Res.* 92(C10):10767–10776. doi:10.1029/JC092iC10p10767
- Jan, Y., and W.A. Jury. 1996. Characterizing the dependence of gas diffusion coefficient on soil properties. *Soil Sci. Soc. Am. J.* 60:66–71. doi:10.2136/sssaj1996.03615995006000010012x
- Jordan, A.B., J.K. MacCarthy, P.H. Stauffer, G.A. Zywloski, M.A. Person, and D.N. Anderson. 2012. Simulation of radionuclide gas breakthrough from underground nuclear explosions. In: Proceedings of the 2012 Monitoring Research Review: Ground Based Nuclear Explosion Monitoring Technologies, Albuquerque, NM. 18–20 Sept. 2012. Vol. 2. Natl. Nucl. Secur. Admin., Washington, DC, p. 625–634.
- King, D.B., and E.S. Saltzman. 1995. Measurement of the diffusion coefficient of sulfur hexafluoride in water. *J. Geophys. Res.* 100(C4):7083–7088. doi:10.1029/94JC03313
- Kwicklis, E.M., A.V. Wolfsberg, P.H. Stauffer, M.A. Walvoord, and M.J. Sully. 2006. Multiphase, multicomponent parameter estimation for liquid and vapor fluxes in deep arid systems using hydrologic data and natural environmental tracers. *Vadose Zone J.* 5:934–950. doi:10.2136/vzj2006.0021
- Lowrey, J.D., S.R. Biegalski, A.G. Osborne, and M.R. Deinert. 2013. Subsurface mass transport affects the radon signatures that are used to identify clandestine nuclear tests. *Geophys. Res. Lett.* 40:111–115. doi:10.1029/2012GL053885
- Massmann, J.W., and D.F. Farrier. 1992. Effects of atmospheric pressures on gas transport in the vadose zone. *Water Resour. Res.* 28:777–791. doi:10.1029/91WR02766
- Mihopoulos, P.G., M.T. Suidan, G.D. Sayles, and S. Kaskasian. 2002. Numerical modeling of oxygen exclusion experiments of anaerobic bioventing. *J. Contam. Hydrol.* 58:209–220. doi:10.1016/S0169-7722(02)00037-2
- Millington, R.J., and J.P. Quirk. 1961. Permeability of porous solids. *Trans. Faraday Soc.* 57:1200–1207. doi:10.1039/TF9615701200
- Morrison, F.A. 1973. Transient multiphase multicomponent flow in porous media. *Int. J. Heat Mass Transfer* 16:2331–2342. doi:10.1016/0017-9310(73)90018-5
- Neeper, D.A., and P.H. Stauffer. 2012. Transport by oscillatory flow in soils with rate-limited mass transfer: 1. Theory. *Vadose Zone J.* 11(2). doi:10.2136/vzj2011.0093
- Nilson, R.H., and K.H. Lie. 1990. Double-porosity modeling of oscillatory gas motion and contaminant transport in a fractured porous medium. *Int. J. Numer. Anal. Methods Geomech.* 14:565–585. doi:10.1002/nag.1610140804
- Nilson, R.H., P.E. Peterson, K.H. Lie, N.R. Burkhard, and J.R. Hearst. 1991. Atmospheric pumping: A mechanism causing vertical transport of contaminated gases through fractured permeable media. *J. Geophys. Res.* 96:21933–21948. doi:10.1029/91JB01836

- Oldenburg, C.M., and A.J.A. Unger. 2003. On leakage and seepage from geologic carbon sequestration sites. *Vadose Zone J.* 2:287–296. doi:10.2136/vzj2003.2870
- Pirkle, R.J., D.E. Wyatt, V. Price, and B.B. Looney. 1992. Barometric pumping: The connection between the vadose zone and the atmosphere. In: *Proceedings of the Focus Conference on Eastern Regional Ground Water Issues*, Boston, MA. 13–15 Oct. 1992. Natl. Ground Water Assoc., Westerville, OH.
- Sander, R. 2013. Henry's law constants. In: P.J. Linstrom and W.G. Mallard, editors, *NIST Chemistry WebBook. NIST Standard Ref. Database 69*. Natl. Inst. of Standards and Technol., Gaithersburg, MD. <http://webbook.nist.gov> (accessed 1 May 2013).
- Scanlon, B.R., J.P. Nicot, and J.W. Massmann. 2001. Soil gas movement in unsaturated systems. In: A.W. Warrick, editor, *Soil physics companion*. CRC Press, Boca Raton, FL. p. 297–391. [http://www.beg.utexas.edu/staffinfo/Scanlon\\_pdf/ScanlonSoilPhysComp02.pdf](http://www.beg.utexas.edu/staffinfo/Scanlon_pdf/ScanlonSoilPhysComp02.pdf) (accessed 1 June 2013).
- Schery, S.D., D.H. Gaeddert, and M.H. Wilkening. 1982. Transport of radon from fractured rock. *J. Geophys. Res.* 87(B4):2969–2976. doi:10.1029/JB087iB04p02969
- Stauffer, P.H., K.H. Birdsell, M.S. Witkowski, and J.K. Hopkins. 2005. Vadose zone transport of 1,1,1-trichloroethane: Conceptual model validation through numerical simulation. *Vadose Zone J.* 4:760–773. doi:10.2136/vzj2004.0120
- Stauffer, P.H., J.A. Vrugt, H.J. Turin, C.W. Gable, and W.E. Soll. 2009. Untangling diffusion from advection in unsaturated porous media: Experimental data, modeling, and parameter uncertainty assessment. *Vadose Zone J.* 8:510–522. doi:10.2136/vzj2008.0055
- Stump, B.W., D.C. Pearson, and R.E. Reinke. 1999. Source comparisons between nuclear and chemical explosions detonated at Rainier Mesa, Nevada Test Site. *Bull. Seismol. Soc. Am.* 89:409–422.
- Sun, Y., and C.R. Carrigan. 2014. Modeling noble gas transport and detection for the Comprehensive Nuclear-Test-Ban Treaty. *Pure Appl. Geophys.* 171:735–750. doi:10.1007/s00024-012-0514-4
- Thordarson, W. 1965. Perched ground water in zeolitized-bedded tuff, Rainier Mesa and vicinity, Nevada Test Site, Nevada. Open-File Rep. TEI-862. USGS, Reston, VA.
- Tompson, A.F.B., C.J. Bruton, G.A. Pawloski, D.K. Smith, W.L. Bourcier, D.E. Shumaker, et al. 2002. On the evaluation of groundwater contamination from underground nuclear tests. *Environ. Geol.* 42:235–247. doi:10.1007/s00254-001-0493-8
- Tong, C. 2005. PSUADE user's manual. Rep. LLNL-SM-407882. Lawrence Livermore Natl. Lab., Livermore, CA.
- Townsend, D.R., M. Townsend, and B.L. Ristvet. 2007. A geotechnical perspective on post-test data for underground nuclear tests conducted in Rainier Mesa. Rep. DTRIAC-SR-07-002-DOE/MV/25946-269. Defense Threat Reduction Agency, Kirtland AFB, NM.
- Witherspoon, P.A., J.S.Y. Wang, K. Iwai, and J.E. Gale. 1980. Validity of cubic law for fluid flow in a deformable rock fracture. *Water Resour. Res.* 16:1016–1024. doi:10.1029/WR016i006p01016
- Wyatt, D.E., D.M. Richers, and R.J. Pirkle. 1995. Barometric pumping effects on soil gas studies for geological and environmental characterization. *Environ. Geol.* 25:243–250. doi:10.1007/BF00766753
- Zyvoloski, G.A. 2007. FEHM: A control volume finite element code for simulating subsurface multi-phase multi-fluid heat and mass transfer. Rep. LA-UR-07-3359. Los Alamos Natl. Lab., Los Alamos, NM.
- Zyvoloski, G.A., B.A. Robinson, Z.V. Dash, and L.L. Trease. 1997. Summary of the models and methods for the FEHM application: A finite element heat- and mass-transfer code. Rep. LA-13307-MS. Los Alamos Natl. Lab., Los Alamos, NM.